JOURNAL OF APPLIED ELECTROCHEMISTRY 25 (1995) 462–471

Oxygen evolution on electrochemically generated cobalt spinel coating

E. POTVIN, L. BROSSARD

Institut de Recherche d'Hydro-Québec (IREQ), 1800 montée Ste-Julie, Varennes, Québec, Canada J3X 1S1

Received 24 February 1994; revised 1 October 1994

The oxygen evolution reaction (OER) has been investigated in 40 wt % KOH at 80 °C on a thick cobalt oxide coating obtained by potential cycling of a cobalt electrode for 0, 2, 4, 10 and 17 h in the same electrolyte with and without dissolved strontium. The kinetic parameters of the OER were determined after preanodization for 1 h at 1 A cm^{-2}. Improved electrocatalytic activity for the OER, better mechanical strength of the coating and lower variation of the oxygen overpotential with time were noticed up to 70 h of polarization as the coating built up in the presence of dissolved strontium in the electrolyte. The beneficial effect of dissolved strontium on the electrocatalytic activity is ascribed to the accumulation of Co_3O_4, which results in a lower Tafel slope for the OER.

1. Introduction

Anode overpotential is one of the major contributions to the cell voltage of industrial water electrolysers. Dioxide, perovskite and spinel type oxides are the most suitable electrode materials for the oxygen evolution reaction (OER) in hot alkaline media; among the possible oxide catalysts, complex oxides with a spinel structure offer the greatest interest. Anodes of the cobaltite spinel type, Co_3O_4, are generally stable under OER and show a good performance [1]. The spinel type Co_3O_4 was prepared by thermal decomposition, the freeze-dry method [2–7], spray pyrolysis [8] or different electrochemical techniques [9–12].

The stoichiometric oxide Co_3O_4 is a normal spinel. Its cation distribution is $Co^{2+}[Co_2^{3+}]O_4^{2-}$ where Co^{2+} and Co^{3+} are in the tetrahedral and octahedral environments, respectively [13]. This oxide is a p-type semiconductor [14] with a high electrical resistivity [6]. Doped with Li [6, 15], it offers a good performance for OER, a fact that is attributed to the lower electrical resistivity and larger Co^{3+} ion concentration in the tetrahedral site of the oxide with Li doping. The conductivity of Co_3O_4 is reported to be closely linked to the preparation procedure because of the change in the composition of the oxide on the surface [16–19]. Quite an acceptable performance for the OER was also reported for Co_3O_4 doped with Ru, Ir, Rh species [3] and Fe [5]. In addition, good electrocatalysts were obtained from mixed oxides of Co_3O_4 and RuO_2 [20].

Unsuccessful attempts have been made to prepare perovskite type $SrCoO_{3-x}$ by the thermal decomposition method [5] and by thermal synthesis from oxides and/or carbonates at elevated temperature [21]. However, Balej [5] produced a mixture of $SrCO_3 + Co_3O_4$ with a fairly high electrocatalytic activity for the OER, although it cannot be ruled out that this high activity may be attributed to a positive influence of the Sr^{2+} ions.

Different electrochemical techniques can be used to obtain an electrolytically active thick cobalt oxide film for the OER [4, 9–12]. For example, the application of a repetitive square-wave potential signal to cobalt electrodes in alkaline solutions results in the formation of an amorphous Co_3O_4 spinel [10]; this spinel oxide was identified by *ex situ* i.r. and X-ray diffraction (after thermal treatment, in the latter case). The authors concluded that Co_3O_4 accumulation is possible by a side reaction during the cathodic half-cycle but the reason for the improved OER remains hidden. A similar approach was adopted to generate a thick hydrated oxide film on a cobalt electrode and a linear dependence of the current density on the amount of reducible oxide at a given overpotential was reported [11]. Burke *et al.* [12] subjected a cobalt electrode in base to a repetitive triangular potential sweep and again a thick cobalt hydrous oxide film was generated. In this case, a slight increase in the OER rate combined with a decrease in the Tafel slope was reported. It is also relevant to report that a highly porous cobalt oxide electrode was produced by the reactive electrodeposition of cobalt in the presence of bubbling oxygen [9]. The high performance of this electrode is due to the unique porous structure of the material and its very high electrical conductivity.

The present work deals with the formation of thick cobalt oxide coatings obtained through potential cycling of a cobalt electrode in 40 wt % KOH at 80 °C in the presence of dissolved strontium for the purpose of improving the OER in such solutions. It is shown that the addition of dissolved strontium during the oxide film buildup improves the mechanical stability of the coating and lowers the overpotential for the OER. Both the morphology and

0021-891X 1995 Chapman & Hall

the composition of the coatings are affected by the presence of strontium.

2. Experimental details

A conventional electrochemical cell of polysulfone was used. The main compartment was kept at a constant temperature of 80 °C by means of a Haake W26 water thermostatic bath. A large area nickel electrode served as the counter electrode. The 0.157 cm^2 working electrode consisted of a cobalt wire (99.997%, AESAR) fixed in a vertical position 0.5 mm from the Luggin capillary which was connected to the outside reference electrode of Hg/HgO/40 wt % KOH held at 25 °C. The reversible potential for the HER was measured by bubbling hydrogen against a platinized platinum electrode immersed in 40 wt % KOH; at 25 °C, it was −918 mV vs RHE while the equilibrium potential for the OER was 270 mV. The solution was deaerated by nitrogen bubbling before and during the experiments. The 40 wt % KOH solutions were prepared from a Fisher certified ACS reagent grade using Nanopure water (18 MΩ resistivity).

The cobalt wire electrodes were polished with 0.3 μm of alumina paste and rinsed with distilled water. The samples were immersed in a deaerated 40 wt % KOH solution at 80 °C. Growth of the oxide coating on the cobalt wire electrodes was achieved by potentiodynamic cycling at a scan rate of 0.03 V s^{-1} with cathodic and anodic potential limits of 0.07 and 1.54 V vs RHE, respectively; thus, hydrogen and oxygen gas evolution and reduction of Co(II) to Co(0) were avoided. The potentiodynamic cycling conditions were borrowed from [12]. The potential was cycled continuously for 1, 2, 4, 10 and 17 h in the absence or presence of 250 ppm of dissolved strontium in 40 wt % KOH solutions at 80 °C. Strontium was introduced by dissolving $Sr(NO_3)_2$ (99.995%, Aldrich Chemicals) in the electrolyte prior to the

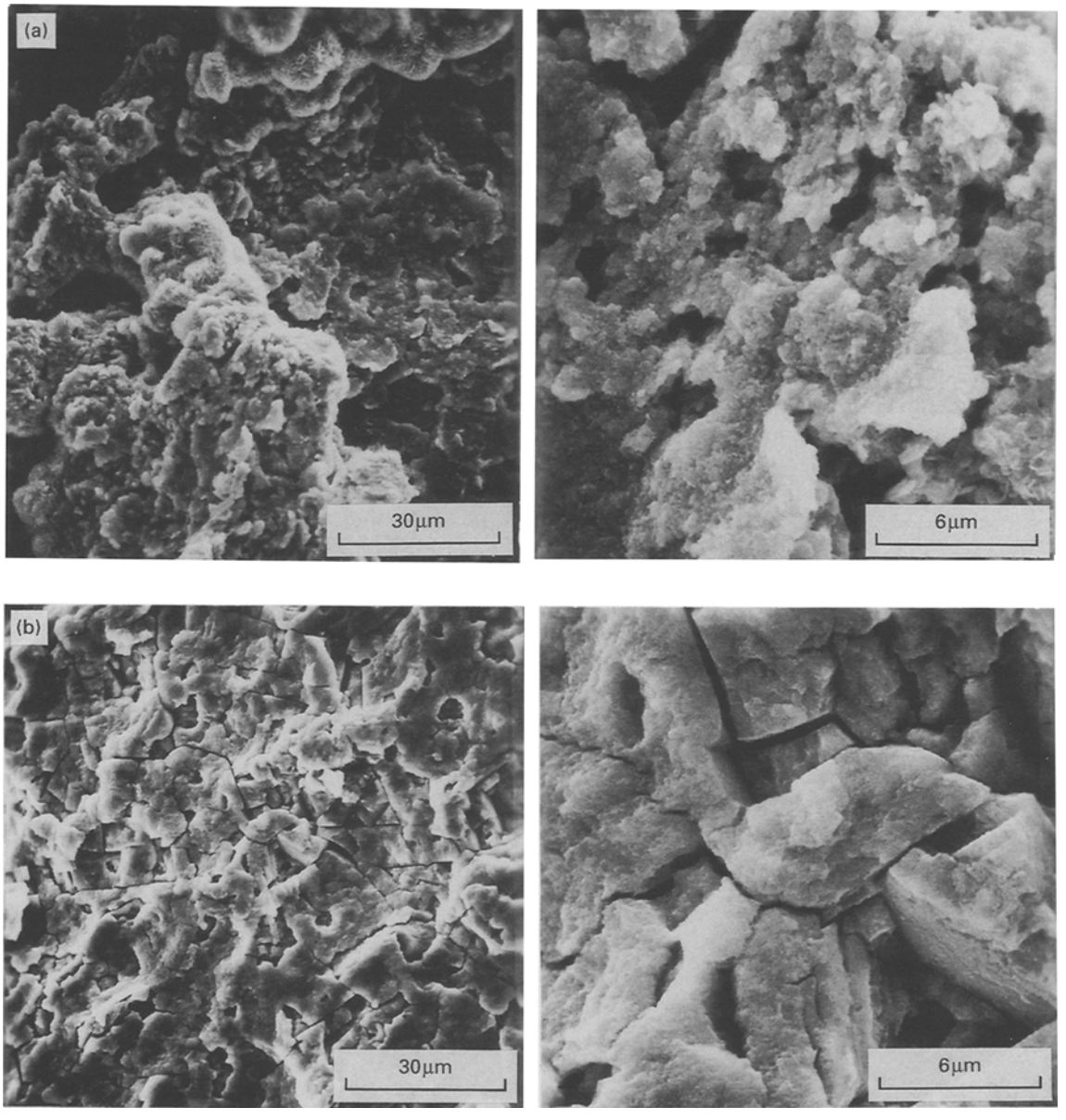

Fig. 1. SEM pictures of cobalt electrodes after 17 h of potential cycling at 0.03 V s^{-1} in 40 wt % KOH at 80 °C. Potential scan limits: 0.07 and 1.54 V vs RHE: (a) in the absence of dissolved strontium and (b) in the presence of 250 ppm dissolved strontium from $Sr(NO_3)_2$.

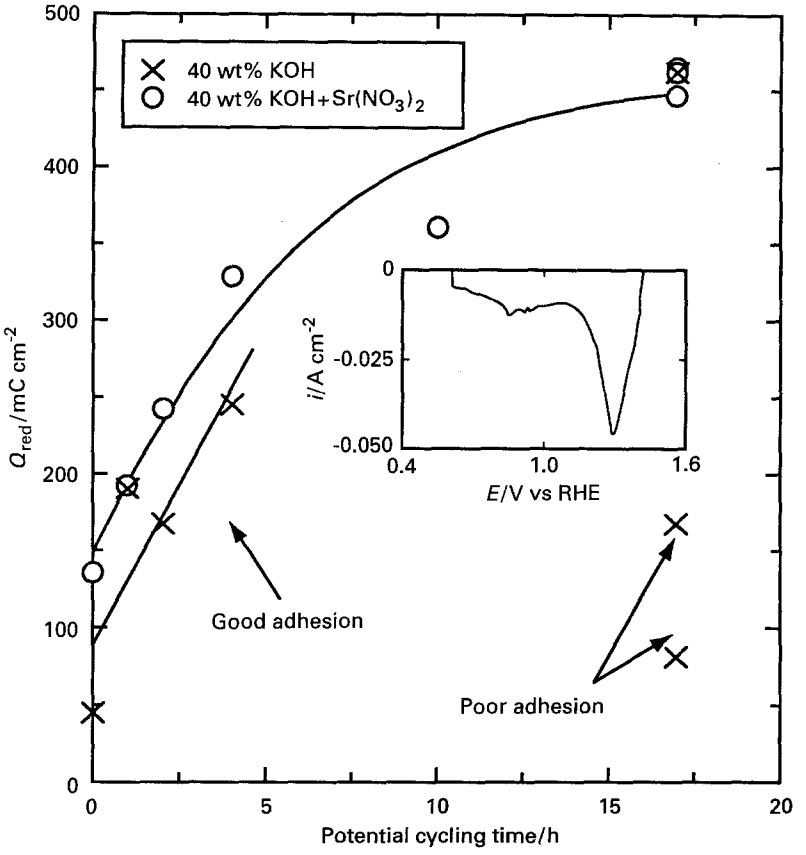

Fig. 2. Cathodic voltammetric charge of active cobalt oxides, Q_{red} against PCT for the cobalt oxide buildup: (×) without dissolved strontium in the electrolyte and (○) with 250 ppm dissolved strontium from $Sr(NO_3)_2$. Insert: a potentiodynamic trace for Q_{red} determination.

experiments. It is relevant to note that dissolution of strontium above 250 ppm was difficult.

Immediately after potentiodynamic cycling, a preanodization current density of $1\,A\,cm^{-2}$ was applied for 1 h. The current density (c.d.) was then reduced galvanostatically from 1 to $10^{-4}\,A\,cm^{-2}$ and the Tafel lines were obtained after correcting the oxygen overpotential (η_{O_2}) for the ohmic drop by the current interruption technique. The current was applied by a PAR 273 galvanostat–potentiostat controlled by an IBM-compatible personal computer.

The coating composition was investigated by X-ray diffraction (XRD), while scanning electron microscopy (SEM) was used to observe the coating morphology. The XRD source was molybdenum K_α. The dissolved strontium content in the electrolyte was determined by optical emission spectroscopy with induced coupled plasma.

3. Results

3.1. *Coating characteristics*

SEM pictures of cobalt electrodes exposed to continuous potentiodynamic cycling for 17 h at a sweep rate of $0.03\,V\,s^{-1}$ are presented in Fig. 1. In the absence of dissolved strontium in a solution of 40 wt % KOH (Fig. 1(a)), a porous structure of the coating is noticed but, when strontium is present,

Table 1. Effect of dissolved strontium on the location of peak potentials with potential cycling time in 40 wt % KOH at 80 °C with sweep rate at 100 mV s^{-1}*

Solutions	*Potential cycling time* /h	A_1 /V_{rhe}	A_1' /V_{rhe}	A_2 /V_{rhe}	A_3 /V_{rhe}	C_1 /V_{rhe}	C_2 /V_{rhe}	C_2' /V_{rhe}	C_3 /V_{rhe}
KOH 40 wt %	0	0.303	–	1.009	–	−0.023	0.819	–	–
	1	0.231	0.287	1.001	–	−0.044	0.849	–	–
	2	0.238	0.287	1.001	–	−0.073	0.819	–	–
	4	0.228	0.288	1.025	–	−0.037	0.847	–	–
	17	0.223	0.278	1.029	–	−0.029	0.847	–	–
KOH 40 wt %	0†	0.294	–	1.042	–	−0.062	–	–	–
+	1†	0.285	–	1.056	–	−0.120	–	–	–
$Sr(NO_3)_2$	2	0.260	–	1.076	1.350	−0.056	0.851	–	1.293
	4	0.255	–	0.988	1.334	−0.051	0.851	–	1.290
	17	0.233	–	0.973	1.338	−0.048	0.852	0.922	1.271

* From voltammograms of Figs 3 and 4.
† A_{Sr} oxidation region is present (Fig. 4a, b).

the structure is completely different (Fig. 1(b)): for 40 wt % KOH with dissolved $Sr(NO_3)_2$, the coating has a more regular morphology, is more compact and contains holes and cracks. Adding strontium to the electrolyte during the growth of oxides allows the formation of deposits (Fig. 1(b)) that offer considerably better adherence and mechanical stability than those formed in the absence of strontium.

The amount of cobalt oxides was estimated from the charge (Q_{red}) involved in the cathodic sweep with potential limits of 0.4 and 1.55 V vs RHE at a potential scan of $0.03\,V\,s^{-1}$; this approach is in accordance with [11] and [12]. The following effects of the potential cycling time (PCT) on Q_{red} (Fig. 2) were observed: (i) Q_{red} increases with the cycling time when dissolved strontium is present during potential cycling; (ii) when strontium is absent, Q_{red} increases almost linearly with the PCT up to 4 h of potential cycling but, after that, it shows nonreproducible variations caused by detachment of the coating due to its poor mechanical strength.

3.2. *Voltammetric behaviour of coatings*

Potentiodynamic traces depicting the behaviour of a cobalt electrode cycled in 40 wt % KOH solution at 80 °C are given in Figs 3 and 4. The locations of the peak current potentials are summarized in Table 1. The solution contained either no strontium (Fig. 3) or 250 ppm dissolved strontium resulting from the addition of $Sr(NO_3)_2$ (Fig. 4).

The initial cycle in the absence of strontium displays a first oxidation peak, A_1, at 0.30 V vs RHE followed by a second, A_2, at 1.01 V vs RHE (Fig. 3(a)). A clearly distinguishable hump precedes A_1. Reduction peaks are also noticed: C_2 at 0.82 V vs RHE and C_1 at −0.02 V vs RHE. The observed presence of an anodic response during the return sweep (ranging from 0.54 to 0.19 V vs RHE) has already been reported for cobalt [22] and can be explained by the breakdown of a protective film in this region of potential.

The main change induced by potential cycling in the absence of dissolved strontium affects the first oxidation peak which shows a doublet, A_1 and A_1', from 1 to 17 h of cycling (Figs 3(b) and (c)). The hump preceding the peak A_1 is ill-defined as the potential cycling time increases. The charge related to the broad oxidation region from 1.1 to 1.54 V vs RHE increases with cycling time, although the latter has practically no influence on the shape of the potentiodynamic curve in this region. An ill-defined cathodic region C_3 is observed after 17 h of potential cycling.

The potentiodynamic behavior of cobalt changes in the presence of dissolved strontium (Fig. 4). Four main features are noticed as the potential is cycled. (i) A large oxidation current in the anodic sweep is observed above 0.49 V for a PCT of 0 h and 1 h. From 2 to 17 h, the current in this region is near zero; this oxidation region is labelled A_{Sr} and is located between 0.49–0.97 V vs RHE for a PCT of 0 h and at 0.61 V vs RHE for a PCT of 1 h. (ii) A third oxidation peak, A_3 (with its conjugated reduction peak C_3), appears prior to the onset of oxygen evolution as the cycle number increases. (iii) There is an

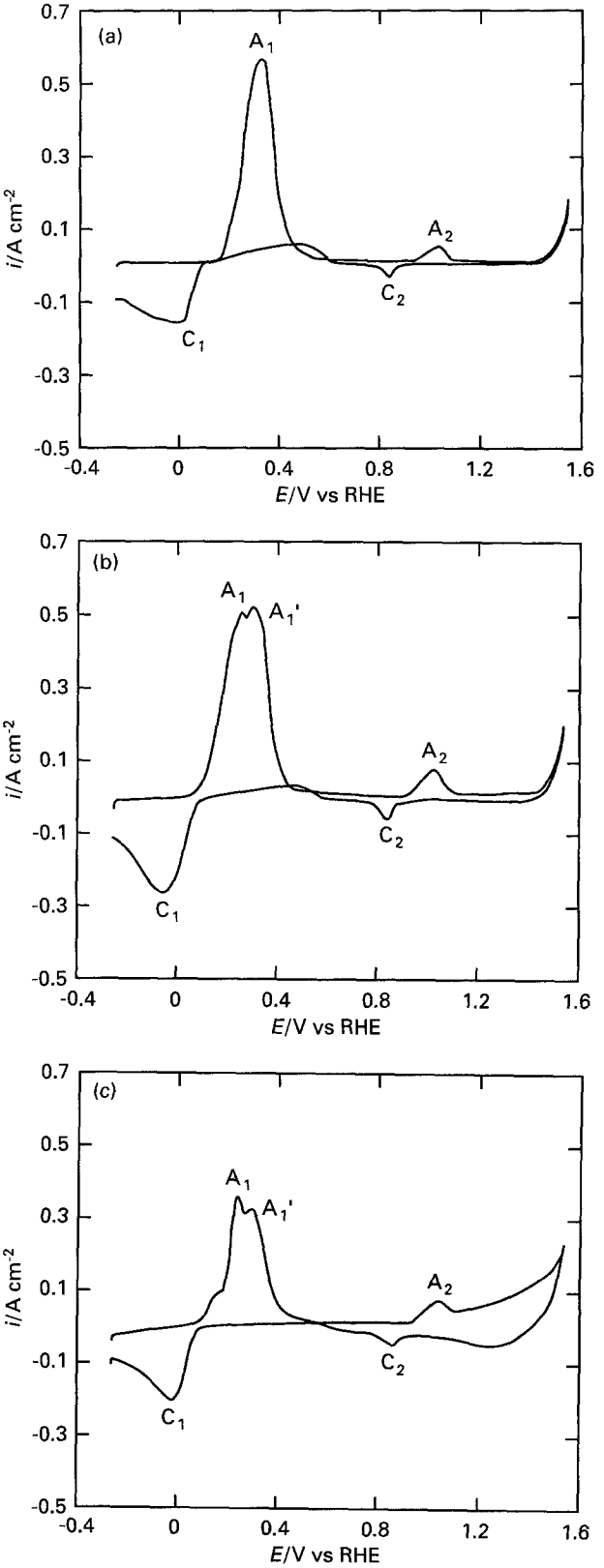

Fig. 3. Effects of potentiodynamic cycling on voltammetric traces for solutions free of dissolved strontium at PCTs of (a) 0 h, (b) 1 h and (c) 17 h (in the absence of film detachment). The other experimental conditions for potential cycling are those of Fig. 1. The voltammograms were recorded at $0.1\,V\,s^{-1}$.

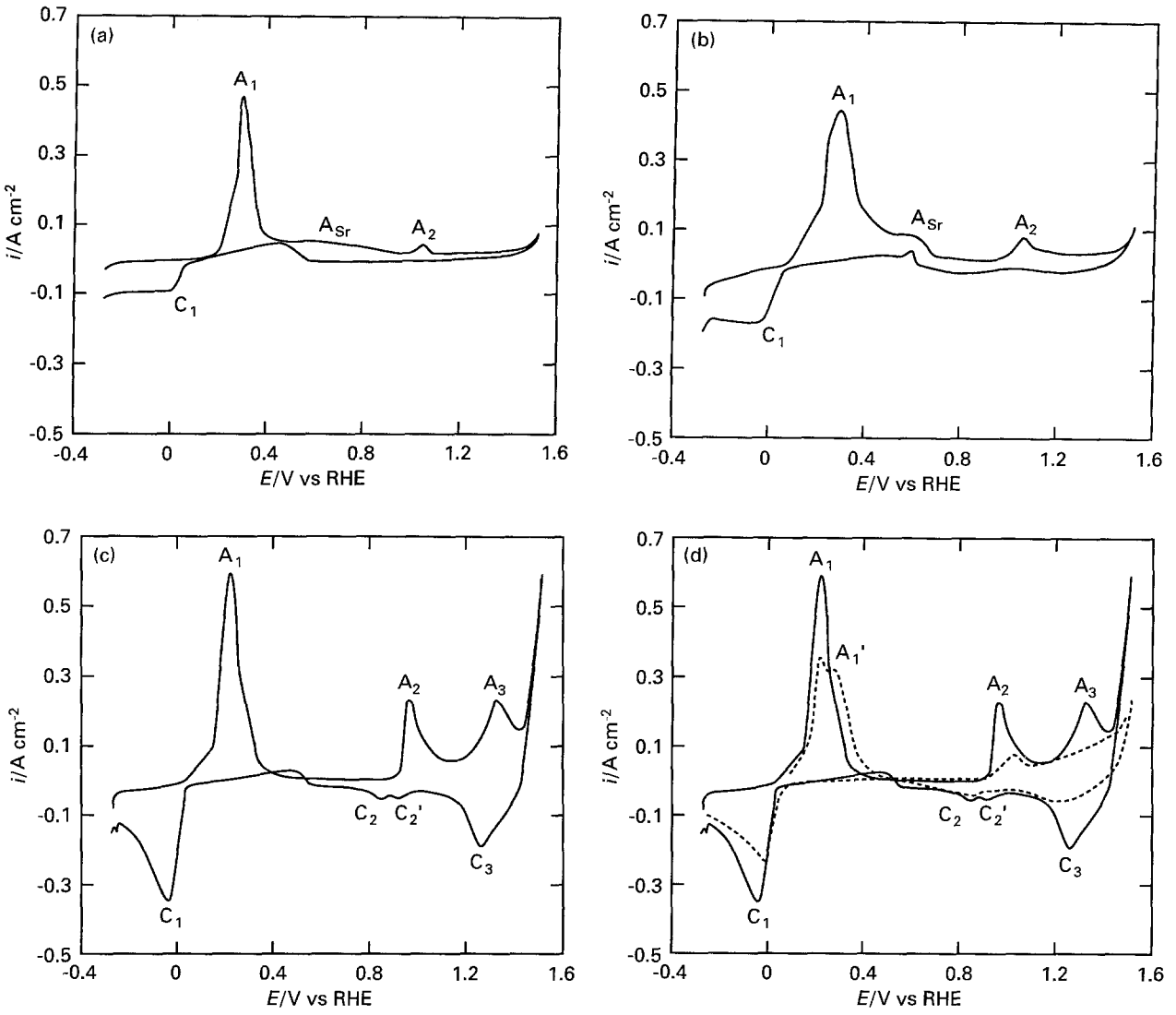

Fig. 4. Effects of dissolved strontium from $Sr(NO_3)_2$ on the potentiodynamic traces after PCTs of (a) 0 h, (b) 1 h, (c) 17 h and (d) Figs. 3(c) and 4(c) combined. The experimental conditions for the potential cycling are those of Fig. 1. The voltammograms were recorded at 0.1 V s^{-1}.

enlargement of oxidation peaks A_2, A_3 as well as the reduction peak C_3 as the number of cycles increases. (iv) The region of Co(II) species formation shows no splitting of peak A_1, regardless of the PCT, but the peak is preceded and followed by a hump.

Comparison of the voltammograms in Figs 3(c) and 4(c) reveals that the formation of cobalt species with a higher valency before the onset of oxygen evolution is favoured when strontium is present in the electrolyte during the oxide coating buildup, as may be seen from the appearance of peaks A_3 and C_3 in Fig. 4(d).

3.3. *Effects of PCT on the OER*

The influence of the PCT on the OER polarization curves of cobalt electrodes in the presence and absence of dissolved strontium is depicted in Fig. 5. The same feature is observed for all solutions: the Tafel slopes of cobalt electrodes obtained after PCTs of 0, 1, 2, 4, 10 and 17 h are characterized by a single linear curve for current densities up to 1 A cm^{-2}. For solutions without dissolved strontium, a slightly detrimental effect of the PCT on the OER performance is noticed (Fig. 5(a)), whereas for solutions containing dissolved strontium (Fig. 5(b)), the effect is very beneficial: the longer the PCT, the easier the reaction.

As anticipated, the OER activity is linked to the amount of active materials, Q_{red}. The kinetic parameters of the OER deduced from the curves in Fig. 5 are summarized in Table 2. The Tafel slopes and the OER overpotential at 1 A cm^{-2} are expressed against Q_{red} in Fig. 6 where the values of Q_{red} are seen to be affected both by the presence of dissolved strontium in the solution and by the PCT.

From $Q_{red} = 50$ to 500 mC cm^{-2}, the Tafel slope varies between 0.9 and 0.93 ($2.3\,RT/F$) for solutions with no dissolved strontium but, in solutions containing strontium, it decreases smoothly from 0.9 ($2.3\,RT/F$) to 0.7 ($2.3\,RT/F$) (Fig. 6(a)). As anticipated from the curves in Fig. 5, the oxygen overpotential at 1 A cm^{-2} does not change markedly with Q_{red} for solutions without dissolved strontium but decreases whenever dissolved strontium is present (Fig. 6(b)).

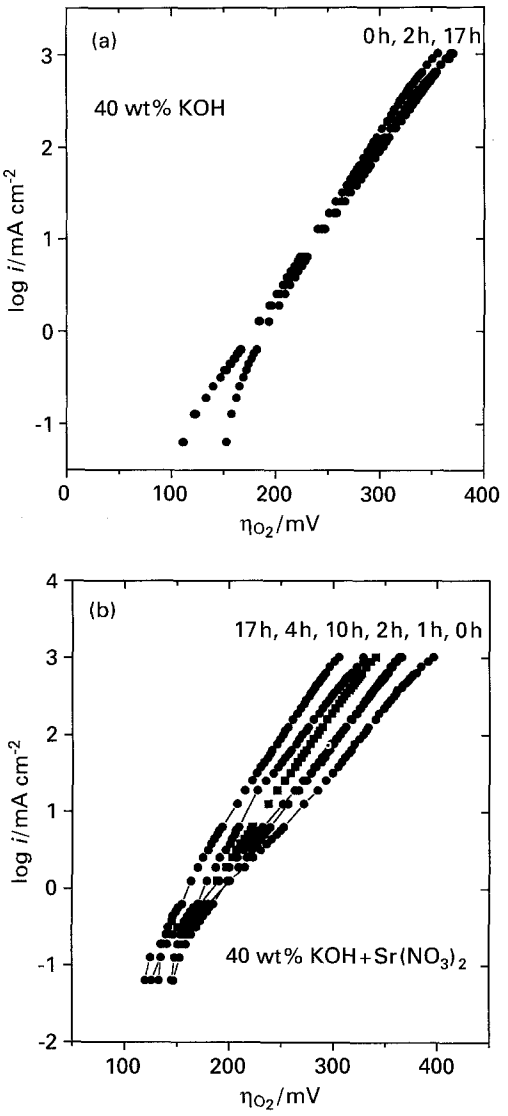

Fig. 5. Polarization curves for the oxygen evolution before and after PCT in solutions (a) without dissolved strontium and (b) with dissolved strontium from $Sr(NO_3)_2$. The other experimental conditions for potential cycling are those of Fig. 1. Preanodization current/time: 1 A cm^{-2}/1 h.

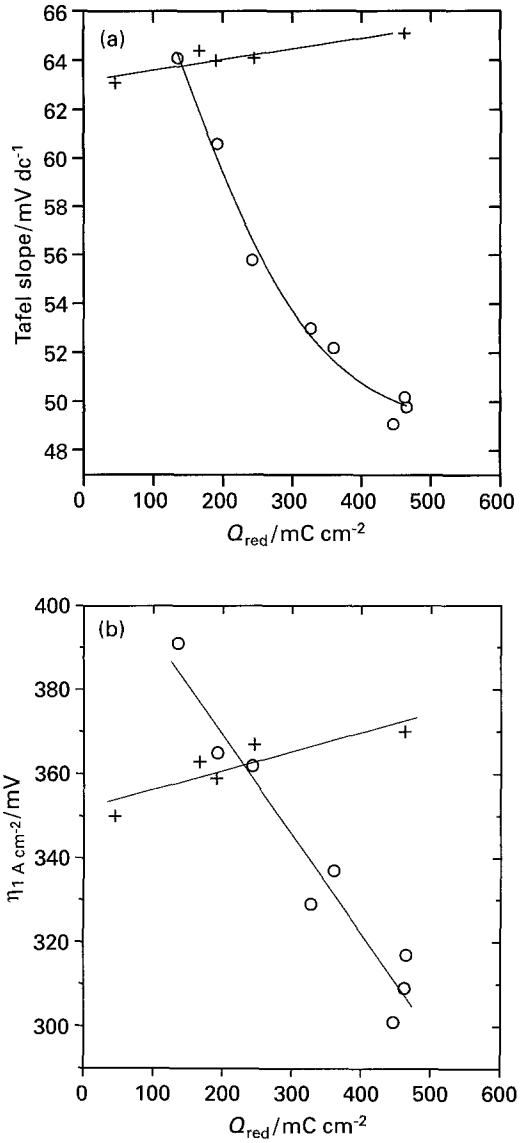

Fig. 6. Tafel slope (a) and oxygen overpotential at 1 A cm^{-2} (b) against Q_{red}. The Tafel slope values are deduced from Fig. 5. Q_{red} is the reduction charge obtained from potentiodynamic traces recorded during the return sweep; it corresponds to the reduction of Co(IV) and Co(III) and possibly Co_3O_4 to Co(II). The sweep rate for the potentiodynamic traces was 0.03 V s^{-1}. Curves: (+) 40 wt % KOH and (○) 40 wt % KOH + $Sr(NO_3)_2$.

Table 2. Tafel parameters of the OER on cobalt electrodes

Solutions	*Potential cycling time* /h	η_{O_2} *A cm*$^{-2}$ /mV	*b* /mV dec^{-1}	Q_{red} /mC cm^{-2}
KOH 40 wt %	0	350	63.1	45
	1	359	64.0	190
	2	363	64.4	166
	4	367	64.1	245
	17	370	65.1	462
KOH 40 wt %	0	391	64.1	135
+	1	365	60.6	192
$Sr(NO_3)_2$	2	362	55.8	242
	4	329	53.0	327
	10	337	52.2	360
	17	301	49.1	446

3.4. *OER overpotential against time*

Figure 7 depicts η_{O_2} at 1 A cm^{-2} against time for cobalt electrodes submitted to a PCT of 17 h prior to the OER. The electrolyte sometimes contained dissolved strontium but, whether it does or not, deactivation is reflected by an increase in η_{O_2} with time and the OER overpotential stabilizes after 40–50 h of polarization. The electrocatalytic activity for the OER is better for solutions containing strontium: η_{O_2} after 72 h of polarization is 337 mV vs RHE compared to 407 mV vs RHE for solutions without strontium.

4. Discussion

To interpret the voltammograms in terms of the formation of different hydroxides and oxides, we considered the thermodynamic data of redox reactions

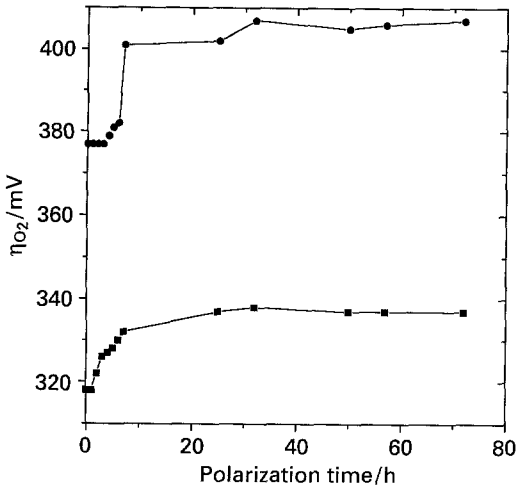

Fig. 7. Oxygen overpotential against time for an oxygen evolution current density of 1 A cm^{-2} on cobalt oxide electrodes after a PCT of 17 h in solutions with or without dissolved strontium. Overpotential values are *IR*-corrected. Curves: (●) 40 wt % KOH, (■) 40 wt % KOH + $Sr(NO_3)_2$.

involving Co(0), Co(II), Co(III) and Co(IV) species in aqueous solutions at 25 °C from [22] and [23]. Account should be taken of the fact that some authors report a slight cathodic shift in redox potential couples with an increase in the base concentration from 1 M to 8–10 M [12, 22] and a rise in the temperature from 35 to 85 °C [24].

Figures 3 and 4 show that the electrochemical behaviour of cobalt in KOH 40 wt % at 80 °C in the presence or absence of dissolved strontium is complex. In the oxidation range of peak A_1, the voltammogram displays two different features: without dissolved strontium, a hump is followed by the splitting of peak A_1 as the PCT becomes larger; with dissolved strontium, the single peak A_1 is preceded and followed by a hump regardless of the PCT.

The voltammogram characteristics in the region of peak A_1 may be explained by the initial formation of $Co(OH)_2$ at that peak [23]. The preceding hump has also been reported and ascribed to the formation of cobaltous hydroxide and the rising portion of peak A_1 to its thickening [22]. Meier *et al.* [25] propose the formation of a sandwich-type structure with an inner $CoOH_{ads}$ monolayer and an outer $Co(OH)_2$ layer. Further oxidation in the Co(II) potential range leads to the formation of a passivating CoO layer sandwiched between the Co metal and the $Co(OH)_2$ film [25–27]. In the present work, the formation of the inner CoO layer can be associated with the splitting of peak A_1 when the electrolyte is free of dissolved strontium (Fig. 3(a)–(c)) or to the hump following peak A_1 when strontium is present (Fig. 4(a)–(c)). Jayaraman *et al.* [24] noticed a marked shoulder on the descending branch of the anodic peak A_1 which they ascribed to the incomplete formation of the CoO film and continuation of the metal dissolution at a reduced rate.

In solutions without dissolved strontium, a second anodic peak A_2 and a small conjugated cathodic peak C_2 are present on the voltammograms for potentials ranging from 1.0–1.03 V vs RHE (Table 1). A third, wide, oxidation region appears at potentials ranging from 1.1 to 1.54 V vs RHE for PCTs of 4 h and 17 h (Fig. 3(c)). The corresponding cathodic process is observed in an ill-defined peak, C_3, in the same figure.

Various cobalt oxides of Co(III) and Co(IV) can form on the metal during anodization between 0.4 and 1.54 V vs RHE in alkaline solutions [22, 23]. There is considerable disagreement about the most likely oxide species produced at different potentials. Grube [28] found three potential arrests in galvanostatic transients of anodic oxidation of Co in alkaline solutions and attributed them to the formation of Co_3O_4, Co_2O_3 and CoO_2. El-Wakkad and Hickling [29] also found three potential arrests but described them as corresponding to CoO, Co_2O_3 and CoO_2. Using cyclic voltammetry, Tikkanen *et al.* [30] observed three anodic current peaks of Co in an alkaline solution and assumed the formation of CoO, Co_3O_4 and $Co(OH)_3$.

Three anodic peaks were identified [24] at 0.5, 0.9 and 1.2 V for electroless Co in 1 N NaOH at 85 °C and attributed to the formation of $Co(OH)_2$/CoO, Co_3O_4 and CoOOH. Haenen *et al.* [31], who studied the potentiodynamic behaviour of Co_3O_4 spinel electrodes in 5 M KOH at 25 °C prepared by the thermal decomposition method, observed three oxidation peaks at 0.875, 1.17 and 1.47 V; from the published standard potentials, they described these peaks as corresponding to a $Co^{2+}/Co^{2.67+}$ transition, a Co^{2+} or $Co^{2.67+}/Co^{3+}$ transition and a Co^{3+}/Co^{4+} or $Co^{2.67+}/Co^{4+}$ transition, respectively. Sato and Ohtsuka [27] studied the anodic oxidation of cobalt in borate buffer alkaline solutions. Their results showed active dissolution, primary, secondary and tertiary passivity and transpassivation. The nature of the anodic oxide films was ascribed to the hydrated CoO in the primary passive region, bilayered oxide CoO/Co_3O_4 in the secondary passive region, and bilayered oxide of CoO/Co_2O_3 in the tertiary passive and transpassive regions. Behl and Toni [22] used cyclic voltammetry and ring-disc electrodes to study the oxidation of cobalt in 0.2 to 8 N KOH solutions at 25 °C. The anodic oxidation of cobalt occurs in the formation of a sandwich-type film of Co/CoO/$Co(OH)_2$ followed by oxidation of the outer $Co(OH)_2$ to Co_3O_4 and CoOOH. Burke *et al.* [12] observed three ill-defined anodic peaks at 1.0, 1.1 and 1.25 V vs RHE and a large anodic background current at potential values above 0.6 V. These peaks were tentatively attributed to the oxidation of Co(II) and Co(III) in species like Co_3O_4, Co_2O_3 and CoOOH. The peak located at 1.48 V vs RHE prior to the onset of oxygen evolution was ascribed to the $CoOOH/CoO_2$ process.

As illustrated by the voltammograms in Figs 3 and 4, electrooxidation of cobalt electrodes at potentials more positive than 0.426 V vs RHE involved oxidation of one of the two Co(II) species of the sandwich-type structure, Co/CoO/$Co(OH)_2$. In the

case of electrodes cycled in a solution free of dissolved strontium, the oxidation process A_2 can be ascribed to oxidation of the outer $Co(OH)_2$ to CoOOH [22, 24, 31]:

$$Co(OH)_{2,outer} + OH^- \longrightarrow CoOOH + H_2O + e^- \quad E^0 = 0.872\,V \text{ vs RHE} \tag{1}$$

For a PCT of 4 to 17 h, peak A_2 was followed by a poorly defined anodic region ranging from 1.1 to 1.54 V vs RHE. First, oxidation of the inner CoO layer to the Co(III) species is the most probable process:

$$CoO_{inner} + OH^- \longrightarrow CoOOH + e^- \quad E^0 = 0.754\,V \text{ vs RHE} \tag{2}$$

According to published thermodynamic data [22, 23], the CoO is oxidized to CoOOH before $Co(OH)_2$. It was proposed by Meier *et al.* [32] that the equilibrium potential of the inner species of the sandwich-type structure may shift toward more positive values, depending on the characteristics of the outer film. Further, the oxidation of Co(III) species to CoO_2 can be considered according to

$$CoOOH + OH^- \longrightarrow CoO_2 + H_2O + e^- \quad E^0 = 1.49\,V \text{ vs RHE} \tag{3}$$

No direct evidence of the anodic formation of Co_3O_4 is seen in the potential range from 0.4 to 1.0 V vs RHE for a PCT of 0 to 17 h; only a small background anodic current is present (Fig. 3(a)–(c)). Kessler *et al.* [10] prepared an amorphous Co_3O_4 spinel coating on a cobalt electrode subjected to a repetitive square-wave potential signal (RSWPS) but did not observe any distinguishable anodic peak corresponding to oxidation of Co(II) species to Co_3O_4 on their untreated cobalt electrode. They concluded that the Co_3O_4 product accumulated as a side cathodic reaction during the main Co(0)/Co(II) and Co(II)/Co(III) redox processes during the RSWPS treatment. Once completed, the oxidation of Co_3O_4 to CoOOH was attributed to a new peak located at 1.3 V vs RHE. Furthermore, a Tafel slope of 50 mV dec^{-1} was observed in the case of the thick Co_3O_4 spinel formed by RSWSP compared to a value of 60 mV dec^{-1} for the untreated cobalt electrode. In the present work, the cathodic accumulation of Co_3O_4 is very unlikely since the Tafel slope is close to $2.303\,RT/F$ for different voltammetric charges (Fig. 6(a)). We therefore concluded that the anodic or cathodic formation of the spinel Co_3O_4 is marginal when the cobalt electrode potential is cycled in 40 wt % KOH at 80 °C for up to 17 h.

It is clear that the anodic processes occurring after formation of the Co(II) species in the presence of dissolved strontium in the electrolyte during the potential cycling of a cobalt electrode are significantly different. For PCTs of 0 h and 1 h, an additional new oxidation region labelled A_{Sr} (Fig. 4(a) and (b)) appears between the anodic formation of Co(II) species (A_1) and the anodic process occurring at peak A_2. As the PCT increases, the disappearance of the oxidation zone A_{Sr} and formation of the well-defined conjugated peaks A_3/C_3 with peak A_3 located at 1.34–1.35 V vs RHE are the dominant features.

According to Meier *et al.* [32], oxidation of the inner CoO film to spinel type Co_3O_4 may proceed via the following reaction in 0.01–2.5 M KOH (free of dissolved strontium):

$$3CoO_{inner} + 2OH^- = Co_3O_{4,inner} + H_2O + 2e^- \quad E^0 = 0.557\,V \text{ vs RHE} \tag{4}$$

The occurrence of Reaction 4 is quite possible in the oxidation region A_{Sr}. Oxidation of part of the bulk of the outer $Co(OH)_2$ film is also possible in the more anodic part of the ill-defined region A_{Sr} obtained for 0 h of potential cycling:

$$3Co(OH)_2 + 2OH^- = Co_3O_4 + 4H_2O + 2e^- \quad E^0 = 0.734\,V \text{ vs RHE} \tag{5}$$

The anodic peak at 0.9 V is attributed [24] to oxidation of the $CoO/Co(OH)_2$ bilayer to Co_3O_4 for electroless Co in 1 M NaOH at 85 °C. In 5 M KOH at 25 °C, the anodic peak located at 0.875 V was related to the $Co^{2+}/Co^{2.67+}$ transition on the Co_3O_4 spinel electrode tested [31]. Moreover, in 0.2–8 N KOH at 25 °C, the anodic peak at 1.0 V vs RHE was linked to oxidation of the outer $Co(OH)_2$ layer to Co_3O_4 [22].

The further oxidation process corresponds to peak A_2, its location being practically the same, with and without the presence of dissolved strontium in the electrolyte. Peak A_2 is attributed to oxidation of the remaining outer $Co(OH)_2$ to CoOOH. The completion of Reaction 1 results in the formation of a sandwich-type structure $Co/Co_3O_4/CoOOH$, according to Meier *et al.* [32]. It is deduced that the process corresponding to peak A_3 is most probably oxidation of the inner spinel Co_3O_4 layer to CoOOH:

$$Co_3O_{4,inner} + OH^- + H_2O = 3CoOOH + e^- \quad E^0 = 1.148\,V \text{ vs RHE} \tag{6}$$

Two anodic processes located in the potential range of 1.17 to 1.48 V vs RHE were reported [10, 12, 22, 24, 28, 31, 32], the first $Co_3O_4/CoOOH$, located at 1.17–1.25 V and the second $CoOOH/CoO_2$ at 1.40–1.48 V vs RHE. In the present work, the location of peak A_3 at 1.34 V vs RHE (Table 1) is consistent with the formation of CoOOH from Reaction 6. Besides, the standard potential of Reaction 3 is more positive than the anodic peak potential A_3, despite the reported shift in redox potential couples with an increase in the base concentration to 8–10 M KOH [12, 22] and the electrolyte temperature from 35 to 85 °C [24]. The lower OH^- concentration and water content expected in the inner-layer film of Co_3O_4 can explain the shift in the equilibrium potential of the couple $Co_3O_4/CoOOH$ toward more positive

values [32]. Further oxidation of CoOOH in CoO_2 is possible after the process linked to peak A_3; however, this reaction overlaps with the onset of the oxygen evolution reaction appearing close to 1.45 V vs RHE (Fig. 4(c)). It may be concluded from potentiodynamic traces that the anodic formation of the Co_3O_4 spinel oxide occurs when the cobalt electrode is potentiodynamically cycled several hours in 40 wt % KOH at 80 °C in the presence of dissolved strontium.

The anodic formation of the Co_3O_4 spinel oxide is supported by X-ray diffractograms. Three such diffractograms obtained with the Mo K_α as source are shown in Fig. 8 for (a) the cobalt substrate, (b) the cobalt oxide deposit on the cobalt substrate and (c) the cobalt oxide powder scraped from the substrate. The presence of a small SrO content [33] or cobalt and strontium oxides [34] cannot be neglected. This is in agreement with the XRD analysis reported for Co_3O_4 spinel electrodes obtained electrochemically by RSWPS treatment after heating [10, 11] and by the thermal decomposition technique [3].

In addition, for a potentiodynamically cycled cobalt electrode in 40 wt % KOH at 80 °C, the Tafel slope for the OER remains close to $2.303\,RT/F$ regardless of a PCT of up to 17 h in the absence of dissolved strontium, but it gradually decreases to $(2/3)\,2.303\,RT/F$ with longer PCT when strontium is dissolved in the electrolyte. The Tafel slope values of the OER on Co_3O_4 electrodes prepared electrochemically and by the thermal decomposition techniques are reported to be around 40–50 mV dec^{-1}. Kessler *et al.* [10] noticed a slope of 50 mV dec^{-1} in the case of the OER on a Co_3O_4 spinel electrode obtained electrochemically by RSWPS treatment

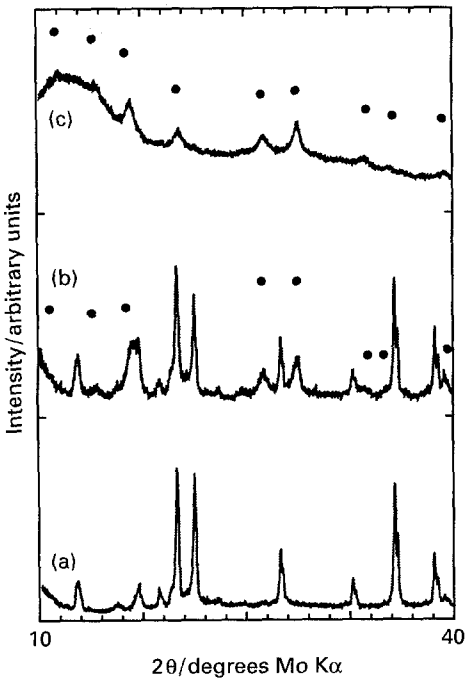

Fig. 8. X-ray diffraction patterns of cobalt oxide electrodes after 17 h PCT in a solution with 250 ppm dissolved strontium from $Sr(NO_3)_2$: (a) cobalt substrate; (b) cobalt oxide coating on the substrate; and (c) cobalt oxide coating scraped off the substrate.

compared to a value of 60 mV dec^{-1} for an untreated cobalt electrode. Burke *et al.* [12] reported a lowering of the Tafel slope for the OER from the uncycled to the potentiodynamically cycled cobalt substrate and attributed the change in the rate-determining step of the OER to the formation of a hydrous cobalt oxide film. Wendt *et al.* [4] studied two different types of Co_3O_4 coatings obtained by thermal decomposition or electrochemically: for both electrodes, a Tafel slope of 40 mV dec^{-1} was obtained in 50 wt % KOH at 90 °C. Meanwhile, an investigation of thin Co_3O_4 films obtained on Ti at 400 °C by spray pyrolysis revealed a Tafel slope in the lower overpotential region of 50 to 40 mV dec^{-1} for 1–8 M KOH solutions at 25 °C [8]. Conway *et al.* [35] observed a slope of 45 mV dec^{-1} at low overpotentials for Co_3O_4 electrodes on Ti and Ni substrates obtained by thermal decomposition. Spinel-type Co_3O_4 electrodes were prepared [3] by the thermal decomposition method on a variety of substrates and a Tafel slope of 45 mV dec^{-1} was found with Fe as substrate compared to 54–64 mV dec^{-1} with Ni, Ti, Nb, Ta and Pt. For Fe/Co_3O_4 electrodes with 5 mol % M (Ru, Ir, Rh), the Tafel slopes of the OER were the same as that reported on Fe/Co_3O_4 electrodes, i.e., 42–48 mV dec^{-1}. However, higher values of the Tafel slope for the OER have been obtained: (i) 60 mV dec^{-1} up to a current density of 0.05 A cm^{-2} for lithium-doped Co_3O_4 [6] and (ii) 60 mV dec^{-1} for Co_3O_4 electrodes prepared by thermal decomposition and doped or not with 5 mol % Fe or Li and doped with Sr, in 10 M KOH at 100 °C [5].

It was postulated that the Co_3O_4 spinel oxide is formed by oxidation of the inner CoO layer according to Reaction 4. The equilibrium potential of the CoO/Co_3O_4 couple shifts toward more positive values, depending on the OH^- concentration and water content in the inner layer [32], the two latter parameters being most likely related to the characteristics of the outer film of $Co(OH)_2$. It is proposed that the presence of strontium in the electrolyte during the potential cycling treatment may promote the formation of a $Co(OH)_2$ film having a porous, open structure [36] so that the transport of ions and the electron transfer are not hindered and oxidation of the inner CoO can proceed easily, that is, close to the standard potential of Reaction 4. The main oxidation chain would be Co(0)/Co(II)/Co_3O_4/Co(III) and, possibly, Co(IV).

By contrast, it is suggested that the potential cycling treatment in the absence of dissolved strontium in the electrolyte results in a not very porous outer $Co(OH)_2$ film, which induces a shift in the equilibrium potential of Reaction 4 toward values eventually more anodic than the potential redox couple CoO/CoOOH and $Co(OH)_2$/CoOOH. The main oxidation chain in these conditions would be Co(0)/Co(II)/CoOOH/ and, possibly, Co(IV).

Cobalt electrodes with an oxide charge built up by potential cycling in an alkaline solution containing dissolved strontium have an oxygen overpotential

of 310 and 337 mV at 1 A cm^{-2} for 1 h and 72 h of polarization, respectively. This is comparable to the performance of $SrCoO_{3-x}$ coating prepared by thermal decomposition and other good electrocatalysts for the OER such as Co_3O_4, $LaNiO_3$, $NiCo_2O_4$ and $La_{0.5}Sr_{0.5}CoO_3$ [1–9].

5. Conclusion

X-ray diffraction has revealed that, when the cycling time is long enough, the presence of dissolved strontium in 40 wt % KOH at 80 °C during oxide film buildup by potential cycling of a cobalt electrode induces the formation of Co_3O_4 spinel. This is supported by the existence of well-defined conjugated peaks A_3/C_3 on the potentiodynamic curves just prior to the onset of the oxygen evolution and by the characteristic value of the Tafel slope for the OER. The presence of strontium also improves the mechanical strength of the coating and the long-time polarization stability, most likely because of the favourable effect of the structure of the deposit. In 40 wt % KOH at 80 °C, these anodes have an oxygen overpotential of 310 and 337 mV at 1 A cm^{-2} for 1 h and 72 h of polarization, respectively.

Acknowledgements

The authors thank the Natural Sciences and Engineering Research Council (NSERC) of Canada for the industrial research fellowship granted to Dr Potvin. Financial support from the Department of Energy, Mines and Resources, Canada, and the Industry Hydrogen Council is also gratefully acknowledged.

References

[1] M. R. Tarasevich and B. N. Efremov, *in* 'Electrodes of Conductive Metallic Oxides', Part A (Edited by S. Trasatti), Elsevier, Amsterdam (1980) pp. 221–59.
[2] R. Boggio, A. Carugati and S. Trasatti, *J. Appl. Electrochem.* **17** (1987) 828.
[3] C. Iwakura, A. Honji and H. Tamura, *Electrochim. Acta* **26** (1981) 1319.
[4] H. Wendt, H. Hofman and V. Plzak, *Mater. Chem. Phys.* **22** (1989) 27.
[5] J. Balej, *Int. J. Hydrogen Energy* **10** (1985) 89.
[6] P. Rasiyah and A. C. C. Tseung, *J. Electrochem. Soc.* **130** (1983) 365.
[7] S. M. Jasem and A. C. C. Tseung, *ibid.* **126** (1979) 1353.
[8] R. N. Singh, J.-F. Koenig, G. Poillerat and P. Chartier, *ibid.* **137** (1990) 1408.
[9] S. P. Jiang and A. C. C. Tseugn, *ibid.* **138** (1991) 1216.
[10] T. Kessler, A. Visintin, M. R. de Chialvo, W. E. Triaca and A. J. Arvia, *J. Electroanal. Chem.* **261** (1989) 315.
[11] M. R. G. de Chialvo and A. C. Chialvo, *Electrochim. Acta* **35** (1990) 437.
[12] L. D. Burke, M. E. Lyons and O. J. Murphy, *J. Electroanal. Chem.* **132** (1982) 247.
[13] B. Cossec, *J. Inorg. Nucl. Chem.* **8** (1958) 483.
[14] D. M. Shub, A. N. Chemodanov and V. V. Shalaginov, *Elektrokhimiya* **14** (1978) 595.
[15] D. B. Hibbert and C. R. Churchill, *J. Chem. Soc., Faraday Trans. 1* **80** (1965) 1984.
[16] M. Hamdani, J.-F. Koenig and P. Chartier, *J. Appl. Electrochem.* **18** (1988) 561.
[17] I. D. Belova, V. V. Shalaginov, B. Sh. Galyamov, Yu. E. Roginskaya and D. M. Shub, *Zh. Neorg. Khim.* **23** (1978) 286.
[18] I. D. Belova, B. Sh. Galyamov, Yu. E. Roginskaya, *Elektrokhimiya* **18** (1982) 777.
[19] L. C. Schumacher and I. B. Holzhueter, *Electrochim. Acta* **35** (1990) 975.
[20] L. D. Burke and M. M. McCarthy, *J. Electrochem. Soc.* **135** (1988) 1175.
[21] Y. Matsumoto, S. Yamada, T. Nishida and E. Sato, *ibid.* **127** (1980) 2360.
[22] W. K. Behl and J. E. Toni, *J. Electroanal. Chem.* **31** (1971) 63.
[23] E. Deltombe and M. Pourbaix, 'Atlas of Electrochemical Equilibria in Aqueous Solutions', Pergamon Press, Oxford (1966) p. 322.
[24] T. R. Jayaraman, V. K. Venkatesan and H. V. K. Udupa, *Electrochim. Acta* **20** (1975) 209.
[25] H. G. Meier, J. R. Vilche and A. J. Arvia, *J. Electroanal. Chem.* **134** (1982) 251.
[26] T. Ohtsuka, PhD thesis, Hokkaido University (1976).
[27] N. Sato and T. Ohtsuka, *J. Electrochem. Soc.* **125** (1978) 1735.
[28] G. Grube and O. Feucht, *Z. Elektrochem.* **28** (1922) 568; V. G. Grube, *ibid.* **33** (1927) 389.
[29] S. E. S. El-Wakkad and A. Hickling, *Trans. Faraday Soc.* **46** (1950) 1820.
[30] M. H. Tikkanen and T. Tuominen, *in* Proceedings 3rd International Congress on Metallic Corrosion, vol. 1, MIR, Moscow (1969) p. 489.
[31] J. Haenen, W. Visscher and E. Barendrecht, *J. Electroanal. Chem.* **208** (1986) 273.
[32] H. G. Meier, J. R. Vilche and A. J. Ariva, *ibid.* **138** (1982) 367.
[33] L.-G. Liu and W. A. Bassett, *J. Geophys. Res.* **78** (1973) 8470.
[34] J.-C. Grenier, S. Ghodbane and G. Demazeau, *Mater. Res. Bull.* **14** (1979) 831.
[35] B. E. Conway and T. C. Lui, *Ber. Bunsenges. Phys. Chem.* **91** (1987) 461.
[36] L. D. Burke and E. J. M. O'Sullivan, *J. Electroanal. Chem.* **117** (1981) 155.